J Solid State Electrochem (2012) 16:1917–1923
DOI 10.1007/s10008-011-1584-4

ORIGINAL PAPER

# Low-temperature behavior of $Li_3V_2(PO_4)_3$/C as cathode material for lithium ion batteries

**Zhiqiang Liu · Xueya Kang · Chengfeng Li · Ning Hua · Tuerdi Wumair · Ying Han**

Received: 29 August 2011 / Revised: 17 October 2011 / Accepted: 25 October 2011 / Published online: 26 November 2011


**Abstract** The electrochemical performance of $Li_3V_2(PO_4)_3$/C was investigated at various low temperatures in the electrolyte 1.0 mol $dm^{-3}$ $LiPF_6$/ethyl carbonate (EC)+diethyl carbonate (DEC)+dimethyl carbonate (DMC) (volume ratio 1:1:1). The stable specific discharge capacity is 125.4, 122.6, 119.3, 116.6, 111.4, and 105.7 mAh $g^{-1}$ at 26, 10, 0, −10, −20, and −30 °C, respectively, in the voltage range of 2.3–4.5 V at 0.2 C rate. When the temperature decreases from −30 to −40 °C, there is a rapid decline in the capacity from 105.7 to 69.5 mAh $g^{-1}$, implying that there is a nonlinear relationship between the performance and temperature. With temperature decreasing, $R_{ct}$ (corresponding to charge transfer resistance) increases rapidly, $D$ (the lithium ion diffusion coefficients) decreases sharply, and the performance of electrolyte degenerates obviously, illustrating that the low-temperature electrochemical performance of $Li_3V_2(PO_4)_3$/C is mainly limited by $R_{ct}$, $D_{Li}$, and electrolyte.

**Keywords** Lithium vanadium phosphate · Low-temperature electrochemical performance · Cathode · Carbon coating · Lithium ion battery

Z. Liu · X. Kang · C. Li · N. Hua · T. Wumair · Y. Han
Xinjiang Technical Institute of Physics and Chemistry,
Chinese Academy of Sciences,
Urumqi, Xinjiang 830011, China

Z. Liu · C. Li
Graduate University of Chinese Academy of Sciences,
Beijing 100049, China

Z. Liu · X. Kang (✉) · C. Li · N. Hua · T. Wumair · Y. Han
Xinjiang Key Laboratory of Electronic
Information Materials and Devices,
Urumqi, Xinjiang 830011, China
e-mail: kangxy@ms.xjb.ac.cn

## Introduction

The environmental issue and energy issue become increasingly prominent, and green renewable energy is increasingly gaining more attention. Because of their high energy density and long cycle life, secondary lithium (Li)-ion batteries are the power sources of choice for modern portable electronic devices. With the application of lithium ion battery becoming more and more popular, the new technical requirements have been put forward. Electric vehicle and aerospace missions, for example, require Li-ion batteries to be capable of operating at high rate charge/discharge and low temperatures (e.g., −20 °C or even lower) with appropriate energy density and power capability. Currently, many efforts have been made to identify the new lithium ion battery cathode materials [1–3].

Since the work of Goodenough and co-workers [4, 5], Li transition metal phosphates have been investigated intensively as cathode materials for lithium batteries among researchers because of their outstanding advantages [3, 6, 7]. As one of the Li transition metal phosphates, the monoclinic $Li_3V_2(PO_4)_3$ has recently attracted widespread interest as cathode materials [8] for its outstanding electrochemical performance with good ionic mobility, high reversible capacity, and relatively high operating voltage [8, 9].

The structure of LVP consists of a 3D framework of slightly distorted $VO_6$ octahedra and $PO_4$ tetrahedra sharing oxygen vertexes [8, 10–12]. Such framework containing corner-shared chains of Li polyhedra and interconnected interstitial space is potentially a fast ionic conductor. In the voltage range of 3.0–4.3 V, it can extract and insert two lithium ions reversibly based on the $V^{3+}/V^{4+}$ redox couple, corresponding to a theoretical capacity of 133 mAh $g^{-1}$.

The intrinsic low electronic conductivity [12] hindered the development of Li transition metal phosphates, until a

landmark work was finished by Chung et al. [3] who enhanced the electronic conductivity with a factor of ~$10^8$ by aliovalent doping. Until now, one of the effective ways to increase the electronic conductivity is using carbon coating strategy [13–15], realized by introducing an organic precursor in the starting materials.

At present, the adaptability of $Li_3V_2(PO_4)_3$ is one of the issues that we are concerned of. Herein, a systematic study to investigate the low temperature electrochemical performances of $Li_3V_2(PO_4)_3$/C was conducted. The sample was synthesized by chelation-assisted carbothermic method using $C_2H_2O_4$ as the chelating reagent [16, 17]. The electrochemical performances of the sample were investigated under various low temperature (26– –40 °C) conditions. The microstructures of the material were also characterized using various microscopic techniques and correlated with their low temperature electrochemical performances.

## Experimental

### Sample preparation

The $Li_3V_2(PO_4)_3$/C (LVP/C) sample was synthesized by chelation-assisted carbothermic method using $C_2H_2O_4$ as the chelating reagent [16, 17]. A stoichiometric amount of $V_2O_5$, $Li_2CO_3$, $NH_4H_2PO_4$ (V/Li/P=2:3:3) and 15 wt.% $C_2H_2O_4$ were ground in agate mortar for 4 h using acetone as the media of dispersant agent. The ground powder was preheated at 320 °C for 6.5 h in a tube furnace using nitrogen atmosphere (flowing 99.99% purity nitrogen) to decompose the $C_2H_2O_4$ and $NH_4H_2PO_4$; 20 wt.% sucrose was added while grinding the powder in mortar and then sintered at 800 °C for 12 h also in a tube furnace using nitrogen atmosphere (flowing 99.99% purity nitrogen).

To evaluate the carbon content in the LVP/C composite, the methodology of residual carbon content measurement was adopted [18]. The prepared LVP/C samples were fired at 600 °C in air for 3 h to burn off the residual carbon. The amount of residual carbon can be calculated as follows:

$$x\% = (816\,y\% + 32)/848 \quad (1)$$

where $x$% is the carbon content and $y$% is the weight variation of LVP/C composite before and after the firing. Based on Eq. 1, we calculated the amount of carbon in the LVP/C sample of 6.3 wt.%.

### Structural and morphological characterization

The crystal structure and morphology were investigated by X-ray diffraction (XRD; RINT-2500 V, Rigaku Co with Cu Kα radiation λ=1.5418Å) and scanning electron microscopy (SEM; ZEISS SUPRA 55VP).

### Electrochemical measurements

To test the electrochemical performances, the cathode was prepared by spreading the cathode slurry (80 wt.% of the active material, 10 wt.% of acetylene black, 10 wt.% of polyvinylidene fluoride dissolved in *N*-methyl-2-pyrrolidone) onto an aluminum foil followed by drying in vacuum at 120 °C for 12 h. The cells (CR2025) were assembled in an argon-filled glove box using lithium metal foil as the counter electrode and a porous polypropylene membrane (Celgard 2400) as the separator. The electrolyte was 1.0 mol $dm^{-3}$ $LiPF_6$ in a mixture of EC, DEC, and DMC (volume ratio 1:1:1).

The electrochemical performances of LVP/C were investigated by using CR2025 coin-type cell in constant temperature and humidity environmental chamber (TH-50, Su Zhou Zhi He). The cells were charged and discharged between 2.3 and 4.5 V on a charge/discharge apparatus (BTS-51, Neware, China) (1 C=150 mA $g^{-1}$). Cyclic voltammetry (CV) and electrochemical impedance spectroscopy (EIS) were conducted by using a CHI650 (Shanghai, China) electrochemical working station. The sinusoidal excitation voltage of EIS was 5 mV and the frequency range was between $10^{-2}$ and $10^5$ Hz.

To test the ionic conductivity of the electrolyte–membrane system [19] under various low temperature conditions, the porous polypropylene membrane (Celgard 2400, 30 μm in thickness) was placed between two same-sized (1.13 $cm^2$) stainless steel blocking electrodes. The electrolyte–membrane system was made into a button cell (CR2025) using the same aforementioned electrolyte and then subjected to ac impedance measurement (the sinusoidal excitation voltage, 5 mV, in the frequency range 10 to $10^5$ Hz) using CHI650 (Shanghai, China) electrochemical working station according to the formula:

$$\sigma_{Li} = l/R_b A \quad (2)$$

where $l$, $R_b$, and $A$ are the thickness, bulk resistance, and area of the film, respectively. Based on Eq. 2, the ionic conductivity of the test electrolyte–membrane system could be calculated. The bulk resistance was determined from the cross point of the ac impedance spectrum at high frequency area and the real axis.

## Results and discussion

### Characterization of $Li_3V_2(PO_4)_3$/C

Figure 1a shows the XRD pattern of LVP/C; the diffraction lines can be attributed to a well-crystallized monoclinic LVP phase with the space group of P21/n. The absence of any other signals indicates there are no high content

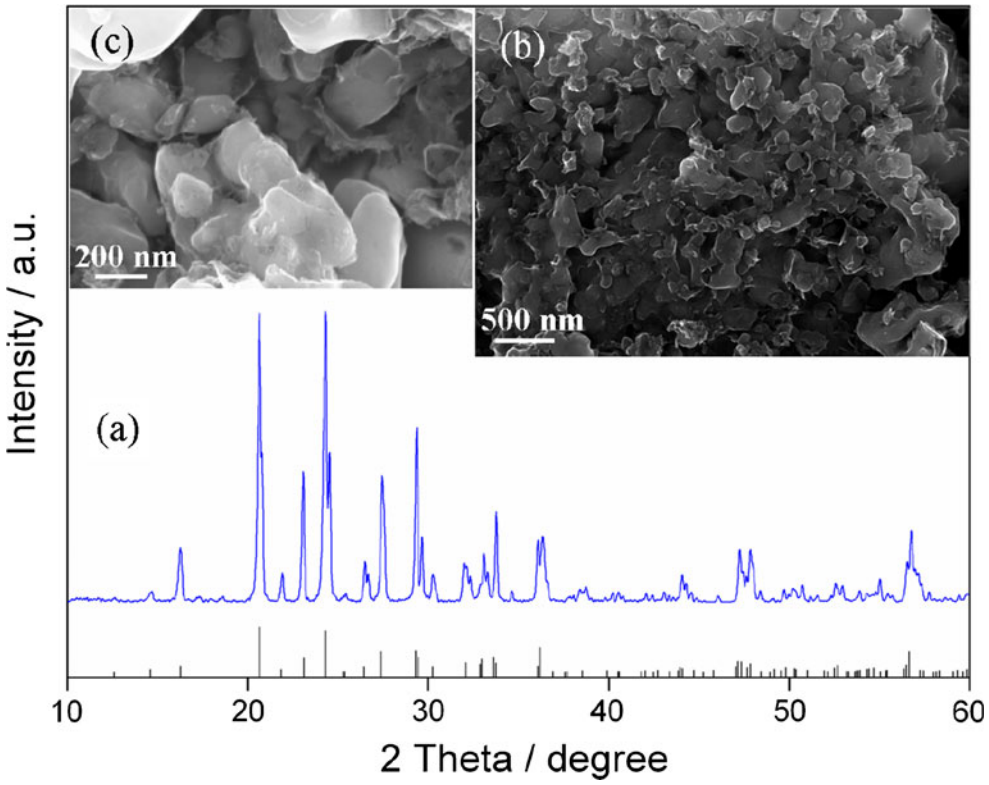


**Fig. 1** **a** XRD patterns of the sample. **b** SEM image of the sample (×27,000). **c** SEM image of the sample (×71,000)

impurities related to $V^{5+}$or $V^{4+}$ compounds and the residual carbon (6.3 wt.%) decomposed from sucrose is amorphous [20, 21] in the composite. The result illustrates the feasibility of our method for the preparation of LVP/C.

The SEM images of the $Li_3V_2(PO_4)_3$/C sample are presented in Fig. 1. The particles of the sample are well crystallized and slightly agglomerated (shown in Fig. 1b). The nano/micron-sized LVP particles present a nearly spherical shape, and they are well interconnected with the help of the carbon network (Fig. 1c). The carbon network can enhance the conductivity of the composite without hindering the insertion/desertion of lithium ions, and it will result in excellent electrochemical performance of $Li_3V_2(PO_4)_3$/C.

## Electrochemical performance of $Li_3V_2(PO_4)_3$/C

The charge/discharge curves of LVP/C are exhibited in Figs. 2 and 3. As seen from the curves, there are three charge flat plateaus (around 3.65, 3.73, and 4.15 V) and three discharge flat plateaus (around 3.51, 3.60, and 4.02 V), exhibiting the characteristic of two-phase behavior between the single phase of $Li_xV_2(PO_4)_3$ ($x$=3.0, 2.5, 2.0, and 1.0).

Figure 2 displays the charge/discharge curves at room temperature (26 °C). The stable specific discharge capacity is 125.4, 122.4, 120.3, 116.5, and 111.3 mAh $g^{-1}$ at 0.2, 1, 2, 5, and 10 C rate, respectively, showing good room temperature performance. The specific discharge capacity is close to the theoretical value, which implies that there are no high content impurities, and the good high current charge/discharge performance with a capacity of 111.3 mAh $g^{-1}$ at 10 C rate, which represents a good electronic conductivity of LVP/C sample, should be attributed to the previously mentioned carbon network. The results are fully consistent with the previous XRD and SEM results.

Figure 3 displays the charge/discharge curves at various temperatures under 0.2 C rate. The stable specific discharge capacities were 125.4, 122.6, 119.3, 116.6, 111.4, 105.7,

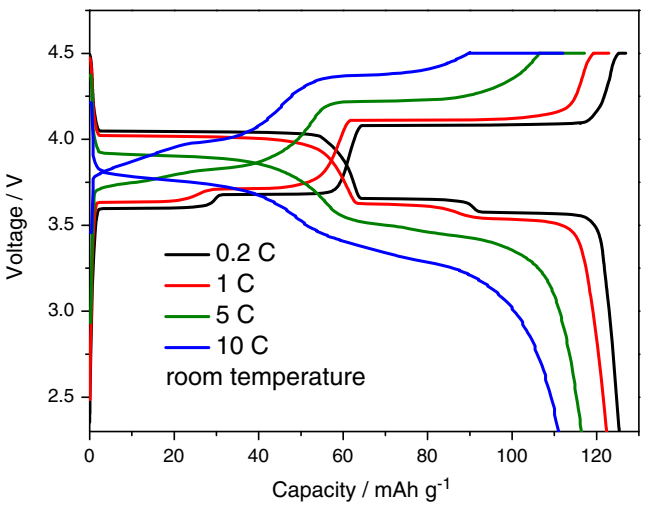


**Fig. 2** Charge/discharge curves of the sample at different *C* rates

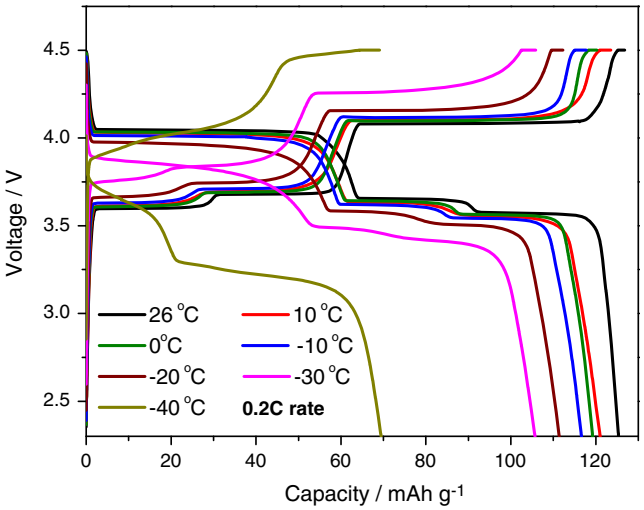


**Fig. 3** Charge/discharge curves of the sample at different temperatures

and 69.5 mAh $g^{-1}$ at 26, 10, 0, −10, −20, −30, and −40 °C, respectively. As seen from the curves, when the temperature decreases from 26 to −30 °C, the capacity decreases slightly from 125.4 to 105.7 mAh $g^{-1}$, and the electrical polarization, as indicated by the voltage difference between the charge (increase) and discharge (decrease) plateaus, increases slowly. It should be noted that, as the operation temperature continues to drop from −30 to −40 °C, there is a rapid decline in the capacity from 105.7 to 69.5 mAh $g^{-1}$ and also a sharp aggravation in the electrical polarization. For a more intuitive representation of this phenomenon, we draw the capacity–temperature dependence under different rates (Fig. 4). As seen from Fig. 4, there is a critical temperature range in the curve. At 0.2 C rate, the critical temperature range is about −30 to −40 °C, and at 1 C rate about −20 to −30 °C. With the rate increasing, the critical temperature range migrates to the high temperature. When the operation temperature drops to the critical temperature range, the electrochemical performance shows an abrupt drop. That is to say, there is a nonlinear relationship, rather than a linear relationship, between the performance and temperature.

According to the literature [22–24], several factors are known to contribute to the poor low temperature performance of lithium ion cells, including: (1) poor electrolyte conductivity, (2) poor lithium transport kinetics in the electrode materials (i.e., bulk), (3) slow diffusion and charge transfer at the electrolyte/electrode interphase, (4) poor wetting and/or transport across the separator material as well as (5) other cell/battery design features. However, in order to understand the nonlinear electrical characteristic presented in the curves of capacity–temperature, more effort has been concentrated on the electrochemical properties of LVP/C.

## Electrochemical properties of $Li_3V_2(PO_4)_3$/C

CV and EIS [25–27] are used to further consider the electrochemical performances of the sample at various temperatures.

Figure 5 illustrates CV curves of the LVP/C sample at room temperature using a scanning rate of 0.1, 0.2, 0.5, and 1 mV $s^{-1}$. In the range of 3.0–4.5 V, there are three oxidation peaks and three corresponding reduction peaks, which are associated with $V^{3+}/V^{4+}$ redox couple. With the sweeping rate rising, the oxidation peak shifts higher and the reduction peak shifts lower.

Figure 6a presents the various temperature Nyquist plots of the sample at the same charge/discharge state, and the fitting equivalent circuit is shown in Fig. 6b [17, 25]. According to the literature [28], $R_e$ represents the solution resistance, $R_f$ signifies the diffusion resistance of Li-ions through the solid electrolyte interface (SEI) layer, and $R_{ct}$

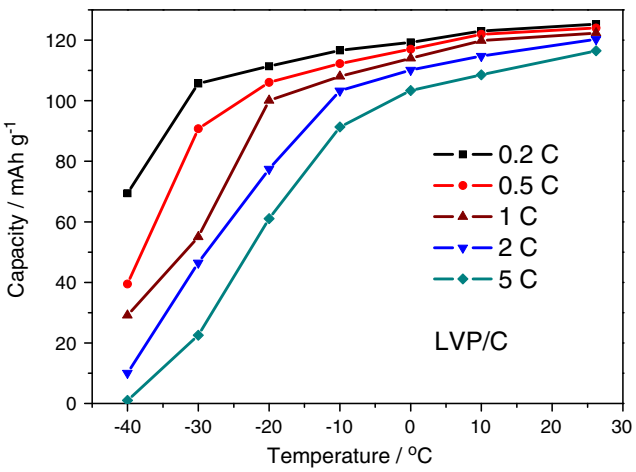


**Fig. 4** Capacity–temperature dependence of the sample at different discharging rates

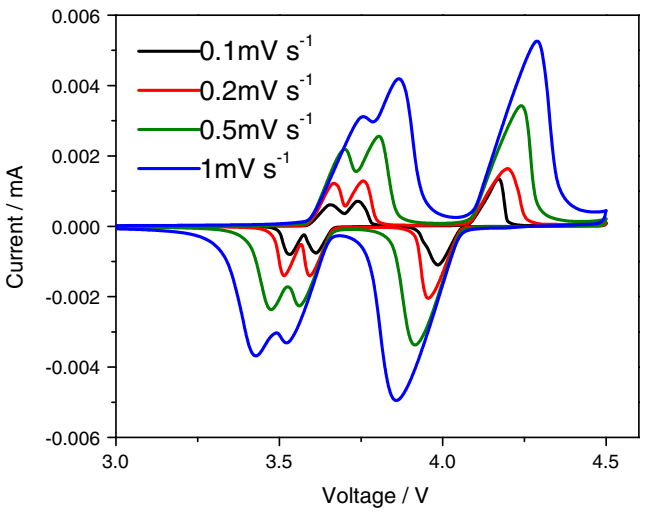


**Fig. 5** CV curves of the sample at different sweeping rates

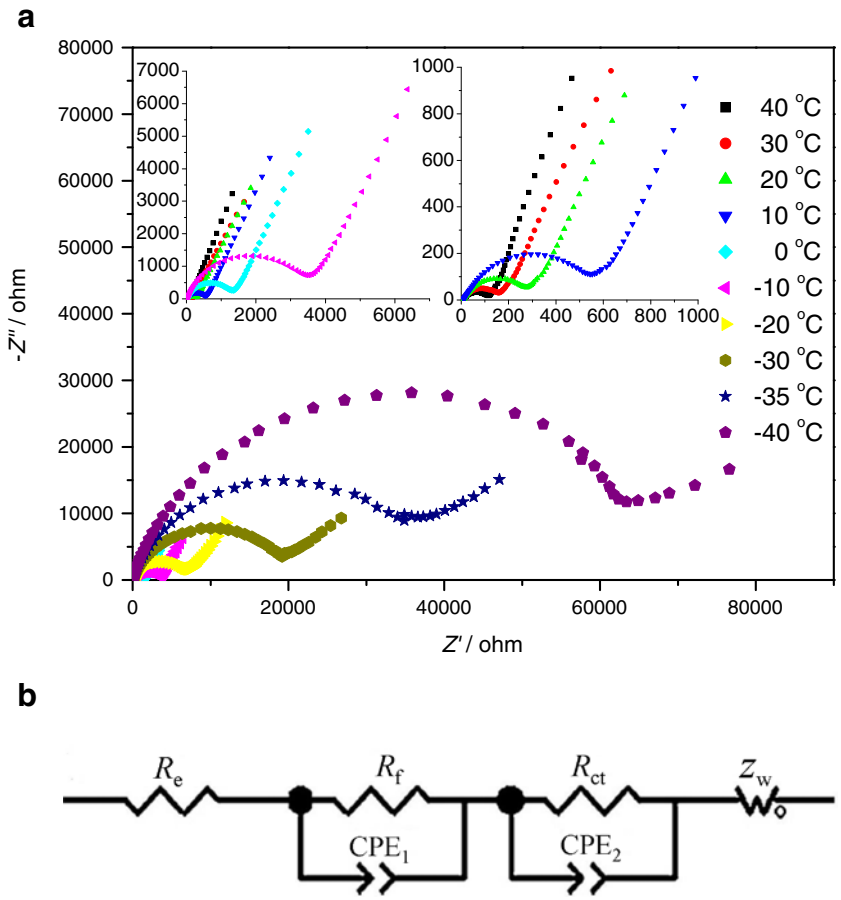


**Fig. 6** **a** Nyquist plots of the sample at different temperatures. **b** Fitting equivalent circuit

corresponds to the charge transfer resistance. $Z_w$ is related to the solid-state diffusion of Li-ions in the active materials corresponding to the slopping line at low frequency. The constant phase element is placed to represent the double-layer capacitance and passivation film capacitance.

The fitting results are listed in Table 1, and the $R_e/R_f/R_{ct}$–temperature curves are displayed in Fig. 7. At the same temperature, $R_e$ is the minimum resistance, $R_{ct}$ is the maximum resistance, and $R_f$ is slightly larger than $R_e$ and much smaller than $R_{ct}$. As the temperature decreases, all the resistances of $R_e$, $R_f$, and $R_{ct}$ increased, while the decreasing of temperature shows a much more pronounced influence on $R_{ct}$. Also, the increase of $R_f$ with the temperature dropping indicates that it is more difficult for $Li^+$ ions to pass through

**Table 1** Electrode kinetic parameters obtained from equivalent circuit fitting of experimental data for LVP/C measured at different temperatures

| | $R_e$ (Ω) | $R_f$ (Ω) | $R_{ct}$ (Ω) | $\sigma$ | $D_{Li}$ ($m^2\ s^{-1}$) |
|---|---|---|---|---|---|
| 40 °C | 8.792 | 13.5 | 55.66 | 175 | $1.436\times10^{-12}$ |
| 30 °C | 8.939 | 16.2 | 83.78 | 257 | $6.238\times10^{-13}$ |
| 20 °C | 10.530 | 23.17 | 158.8 | 318 | $3.810\times10^{-13}$ |
| 10 °C | 11.25 | 30.2 | 345.3 | 395 | $2.304\times10^{-13}$ |
| 0 °C | 12.26 | 69.22 | 889.6 | 559 | $1.070\times10^{-13}$ |
| −10 °C | 13.48 | 158.48 | 3,030 | 886 | $3.955\times10^{-14}$ |
| −20 °C | 15.82 | 650.9 | 7,405 | 1,582 | $1.148\times10^{-14}$ |
| −30 °C | 18.46 | 1,355 | 13,080 | 2,866 | $3.226\times10^{-15}$ |
| −35 °C | 22.83 | 3,245 | 26,080 | 4,929 | $1.034\times10^{-15}$ |
| −40 °C | 30.03 | 5,055 | 51,330 | 6,930 | $5.073\times10^{-16}$ |

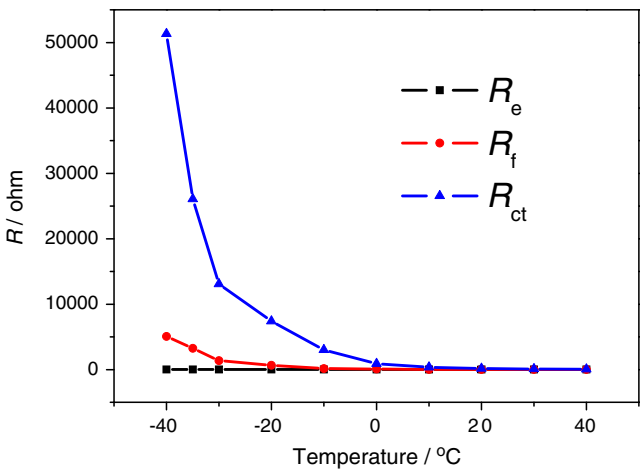


**Fig. 7** $R_e/R_f/R_{ct}$ temperature curves of the sample

the SEI film (on both electrodes [28]) at low temperature; the fact that $R_{ct}$ is much larger than $R_f$ implies that the charge transfer resistance is much larger than the diffusion resistance of Li-ions through SEI at various temperatures. The behavior of lithium anode for Li battery is strongly dependent on its surface chemistry [29]; so, it is clear that the $Li_3V_2(PO_4)_3$/C cathode, not the lithium metal counter electrode, presents a preferred resistive element limiting the behavior of the cell. As shown in Fig. 7, $R_{ct}$ shows an abrupt rise in the range of −30 to −40 °C. This temperature range is consistent with the critical temperature range previously mentioned in Fig. 4. Combined with an analysis of previous test results, a conclusion could be easily drawn that $R_{ct}$ is one of the key factors that limit the low temperature performances of the material, and one of the most effective ways to enhance the low temperature performances may be decreasing the $R_{ct}$ by facilitating the charge transfer reaction, which could be solved by surface modification.

The lithium ion diffusion coefficients ($D_{Li}$) at various temperatures were calculated according to the following equation [25–27]:

$$D_{Li} = R^2T^2/2A^2n^4\,F^4C^2\sigma^2 \quad (3)$$

$$Z' = R_D + R_L + \sigma\omega^{-1/2} \quad (4)$$

where $D_{Li}$ is the lithium ion diffusion coefficient, $R$ is the gas constant, $T$ is the absolute temperature, $A$ is the surface area of the cathode, $n$ is the number of electrons per molecule during oxidization, $F$ is the Faraday constant, $C$ is the concentration of lithium ion, and $\sigma$ is the Warburg factor which could be obtained by Eq. 4.

Figure 8 shows the relationship between $Z'$ and square root of frequency ($\omega^{-1/2}$) in the low-frequency region. The diffusion coefficients of lithium ion ($D_{Li}$) at various temperatures were calculated based on Eqs. 3 and 4 and listed in Table 1. The diffusion coefficient decreased from $1.436\times10^{-12}$ to $5.073\times10^{-16}$ $m^2s^{-1}$ with the temperature dropping from 40 to −40 °C, in the same order as the reported values [30]. Figure 9 shows the relationship between the temperature and $D_{Li}^{-1}$. As seen from the curve, $D_{Li}$ shows an accelerated decline in the range of −30 to −40 °C, which is consistent with the critical temperature range previously mentioned in Fig. 4. The result is also consistent with the recognized nonlinear relationship between $D_{Li}$ and temperature. Combined with an analysis of previous test results, a conclusion could be easily drawn that $D_{Li}$ is one of the key factors that limit the low temperature performances of the material, and lithium ion diffusion channel optimization may be another effective way to enhance the low temperature performances.

Figure 10 shows the ionic conductivities ($\sigma_{Li}$) of the test electrolyte–membrane system at different temperatures. When the temperature decreases from 26 to −40 °C, $\sigma_{Li}$ decreases from 0.098 to 0.006 $Sm^{-1}$; the whole process of decline is relatively gentle despite a slight acceleration below −20 °C. Clearly, the poor ionic conductivity at low temperature also contributes to the drop in low temperature performance of LVP/C.

## Conclusions

NASCION structure $Li_3V_2(PO_4)_3$/C composite is successful synthesized by chelation-assisted carbothermic method

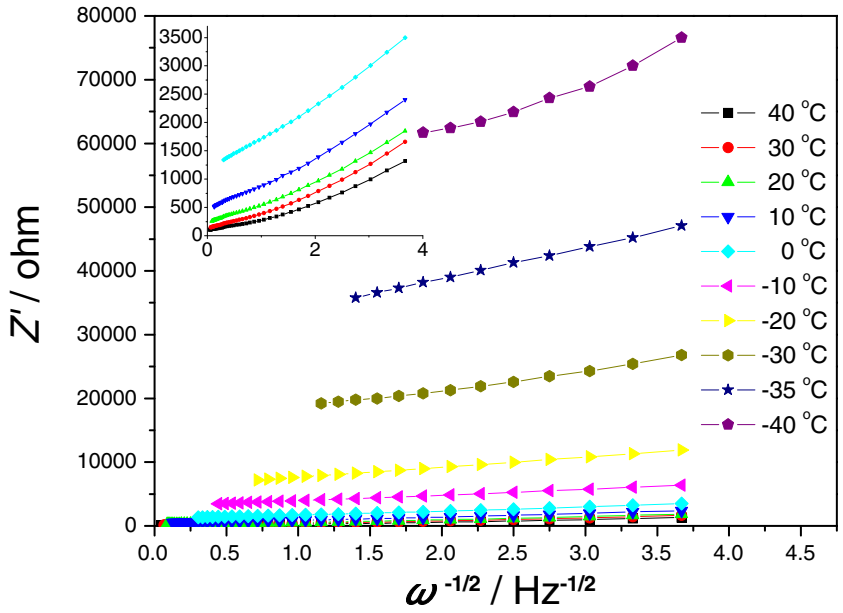


**Fig. 8** The relationship between $Z'$ (ohm) and square root of frequency ($\omega^{-1/2}$) in the low-frequency region

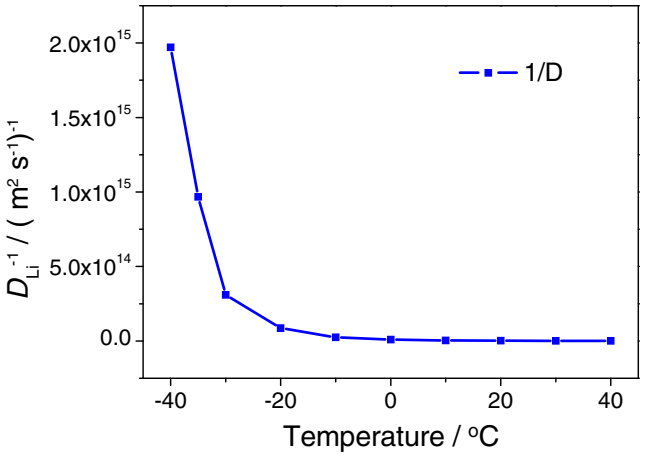


**Fig. 9** The relationship between the temperature and the reciprocal of diffusion coefficient

using $C_2H_2O_4$ as the chelating reagent. The electrochemical performances of the sample are closely related with the temperature: the lower the operation temperature is, the poorer the performances are. There is a nonlinear relationship between the performance and temperature, which is manifested through the critical temperature range in the capacity–temperature curve at the same rate. When the operation temperature decreases to the critical temperature range, the electrochemical performance shows an abrupt drop. As the rate increases, the critical temperature range migrates to high temperature. Experimental results shows that the low temperature electrochemical performance of $Li_3V_2(PO_4)_3/C$ is mainly limited by $R_{ct}$, $D_{Li}$, and electrolyte. The emergence of the critical temperature range should be attributed to the nonlinear change of $R_c$, $D_{Li}$, and $\sigma_{Li}$ with temperature. Surface modification, lithium ion diffusion channel optimization, and electrolyte optimization may be the most effective ways to enhance the low temperature performances.

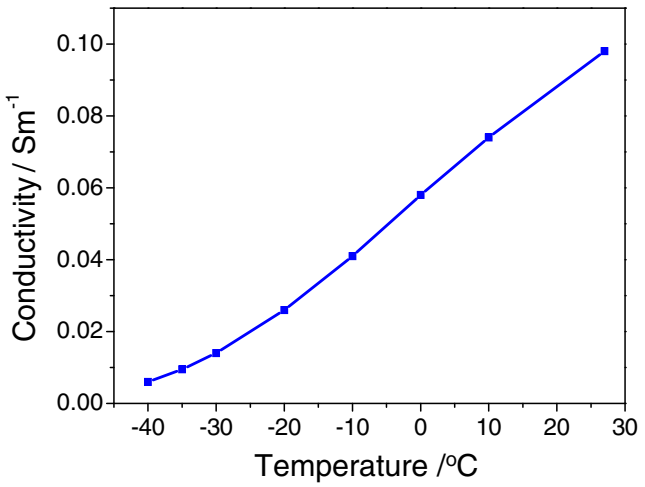


**Fig. 10** The ionic conductivities of the test electrolyte–membrane system at different temperatures

**Acknowledgement** The authors gratefully acknowledge the financial support of the Knowledge Innovation Project of the Chinese Academy of Sciences (No. 20092A401), the West Light Foundation of the Chinese Academy of Sciences (No. XB200919) and the science and technology projects of Urumqi (No. K111410005).

## References

1. Higuchi M, Katayama K, Azuma Y, Yukawa M, Suhara M (2003) J Power Sources 258:119–121
2. Yamada A, Chung SC, Hinokuma K (2001) J Electrochem Soc 148:A224–A229
3. Chung SY, Bloking JT, Chiang YM (2002) Nat Mater 1:123–128
4. Padhi AK, Nanjundaswamy KS, Goodenough JB (1997) J Electrochem Soc 144:1188–1194
5. Padhi AK, Nanjundaswamy KS, Masquelier C, Okada S, Goodenough JB (1997) J Electrochem Soc 144:1609–1613
6. Delacourt C, Poizot P, Tarascon JM, Masquelier C (2005) Nat Mater 4:254–260
7. Thackeray M (2002) Nat Mater 1:81–82
8. Huang H, Yin SC, Kerr T, Taylor N, Nazar LF (2002) Adv Mater 14:1525–1528
9. Saidi MY, Barker J, Huang H, Swoyer JL, Adamson G (2003) J Power Sources 266:119–121
10. Yin SC, Grondey H, Strobel P, Anne M, Nazar LF (2003) J Am Chem Soc 125:10402–10411
11. Yin SC, Grondey H, Strobel P, Huang H, Nazar LF (2003) J Am Chem Soc 125:326–327
12. Yin SC, Strobel PS, Grondey H, Nazar LF (2004) Chem Mater 16:1456–1465
13. Chen Z, Dahn JR (2002) J Electrochem Soc 149:A1184–A1189
14. Belharouak I, Johnson C, Amine K (2005) Electrochem Commun 7:983–988
15. Hua N, Wang CY, Kang XY, Wumair T, Han Y (2010) J Alloys Compd 503:204–208
16. Li CF, Hua N, Wang CY, Kang XY, Wumair T, Han Y (2011) J Solid State Electrochem 15:1971–1976
17. Li CF, Hua N, Wang CY, Kang XY, Wumair T, Han Y (2011) J Alloys Compd 509:1897–1900
18. Rui XH, Li C, Liu J, Cheng T, Chen CH (2010) Electrochim Acta 55:6761–6767
19. Yuan AB, Zhao J (2006) Electrochim Acta 51:2454–2462
20. Shin HC, Cho WI, Jang H (2006) J Power Sources 159:1383–1388
21. Li YZ, Zhou Z, Gao XP, Yan J (2007) Electrochim Acta 52:4922–4926
22. Zhang SS, Xu K, Jow TR (2004) Electrochim Acta 49:1057–1061
23. Ratnakumar BV, Smart MC, Surampudi S (2001) J Power Sources 97–98:137–139
24. Wang CS, Appleby AJ, Little FE (2002) J Electrochem Soc 149: A754–A760
25. Gao F, Tang ZY (2008) Electrochim Acta 53:5071–5075
26. Liu H, Li C, Zhang HP, Fu LJ, Wu YP, Wu HQ (2006) J Power Sources 159:717–720
27. Wang XY, Zhu QA, Zhang YS, Yuan HT, Yan J, Song DY (1999) Chin J Power Sources 23:335–338
28. Zhang SS, Xu K, Jow TR (2006) J Power Sources 159:702–707
29. Aurbach D (2000) J Power Sources 89:206–218
30. Rui XH, Jin Y, Feng XY (2011) J Power Sources 196:2109–2114